

Effect of Crystallinity on Electrostatic Charging in Dry Powder Inhaler Formulations

Jennifer Wong · Philip Chi Lip Kwok · Tim Noakes · Ali Fathi · Fariba Dehghani · Hak-Kim Chan

Received: 10 July 2013 / Accepted: 19 December 2013 / Published online: 24 January 2014
© Springer Science+Business Media New York 2014

ABSTRACT

Purpose This study aimed to characterize inherent charge generated by micron-sized drug-only formulations of amorphous and crystalline salbutamol sulfate (SS).

Methods Amorphous SS was produced by spray-drying whilst crystalline SS was produced by conditioning spray-dried SS with supercritical CO₂ and menthol. Electrostatic charge of the powders was characterized in two ways. Firstly, the charge profile of the aerosols dispersed from an Aerolizer® was measured using a modified Electrostatic Low Pressure Impactor (ELPI™). Secondly, the net charge of the bulk powders generated from tumbling in containers composed of different materials (polyethylene, polyvinyl chloride, Teflon, nylon and stainless steel) was measured by a Faraday pail.

Results Following aerosolization, crystalline SS appeared to show more consistent charging and mass deposition than amorphous SS. In the tumbling experiment crystalline SS had a significant correlation between net charge and work function, which was absent in amorphous SS. This may be due to the long-range crystal packing which was reflected as more predictable charging. In addition, the polarity of charging was attributed to the arrangement of SS molecules in the crystal lattice.

Conclusions The effect of crystallinity on the electrostatic charge behavior of inhalable micron-sized spherical drug particles with well-defined particle size distribution was investigated for the first time. The knowledge gained may assist in the development of optimized inhaled pharmaceutical products.

KEY WORDS crystallinity · dry powder inhaler (DPI) · electrostatic charge · salbutamol sulfate · supercritical fluid

ABBREVIATIONS

AFM	Atomic force microscopy
BET	Brunauer, Emmett and Teller
DPI	Dry powder inhaler
DVS	Dynamic vapor sorption
ELPI	Electrostatic Low Pressure Impactor
FID	Flame ionization detection
GC	Gas chromatography
HPLC	High performance liquid chromatography
RH	Relative humidity
R _q	Root mean squared
scCO ₂	Supercritical CO ₂
SDS	Sodium dodecyl sulfate
SEM	Scanning electron microscopy
SS	Salbutamol sulfate
XRD	X-ray diffraction

INTRODUCTION

Pharmaceutical active ingredients and excipients are likely to retain significant amounts of charge due to high electrical resistivities ($>10^{13} \Omega\text{m}$), with charge relaxation times in the order of minutes to hours, such that retained electrostatic effects would be significant (1). In particular, particles generated from dry powder inhalers (DPIs) undergo triboelectrification from contact with each other and solid surfaces during their manufacture and use. These charges may affect their dosing, aerosol performance, and inhaler retention. Therefore, the selection of

J. Wong · H.-K. Chan (✉)
Advanced Drug Delivery Group, Faculty of Pharmacy
The University of Sydney, Sydney, New South Wales, Australia
e-mail: kim.chan@sydney.edu.au

P. C. L. Kwok
Department of Pharmacology and Pharmacy
Li Ka Shing Faculty of Medicine
The University of Hong Kong, Hong Kong, SAR, China

T. Noakes
Mexichem UK Limited, The Heath Business and Technical Park
Runcom, Cheshire, WA7 4QX, UK

A. Fathi · F. Dehghani
School of Chemical and Biomolecular Engineering
The University of Sydney, Sydney, New South Wales, Australia

formulations and devices with consistent charging at a range of ambient conditions may assist in the development and production of optimized inhalation products.

The past decade of research has found that (i) charging depends on the drug, excipients, and inhaler used (2–4), (ii) respirable particles were estimated to carry charges high enough to affect deposition (2,4), and (iii) the extent and trends of charging were affected by storage and relative humidities (4,5). Overall, charging in DPIs depends on the inhaler design, as well as many physicochemical properties and environmental factors (6,7).

A physicochemical property that may influence charging is crystallinity. Theoretically, amorphous and crystalline surfaces have different crystal packing and surface energy. Hence, their charge transfer behavior may differ. Previous work by Murtomaa *et al.* (8) and Kwok *et al.* (9) have investigated electrostatic charging of amorphous and crystalline particles. Murtomaa *et al.* (8) found that the charging of lactose increased with decreasing crystallinity. On the other hand, Kwok *et al.* (9) observed that amorphous spray-dried salbutamol sulfate (spherical shape) charged more electropositive than crystalline jet-milled salbutamol sulfate (plate-like shape). Particle morphology was not controlled in either study. Therefore, the data were inconclusive and the role of crystallinity on electrostatic charging in DPI formulations remains open for exploration and more controlled studies are needed.

The present study aimed to characterize the inherent charges of spherical amorphous and crystalline salbutamol sulfate (SS) particles generated from aerosolization and tumbling. Amorphous SS was produced by spray-drying, whereas crystalline SS was produced by conditioning spray-dried SS with supercritical CO₂ (scCO₂) and menthol. Electrostatic charge was characterized in two ways: those generated from aerosolization was measured by a modified Electrostatic Low Pressure Impactor (ELPI™), whereas those generated from tumbling in containers of different construction materials was measured by a Faraday pail. Experiments were conducted under ambient conditions with relative humidity (RH) and temperatures that fell within the range 50 ± 5% RH and 22 ± 2°C, respectively.

MATERIALS AND METHODS

Materials

Salbutamol sulfate (99.9% purity) was purchased from Inter-Chemical Co. Ltd., Jiangsu, China; food grade carbon dioxide (99.9% purity) from BOC Ltd., Newcastle, Australia; menthol (99.8% purity) from Sigma-Aldrich, Sydney, Australia; de-ionized water (electrical resistivity > 2 MΩ cm at 25°C) was supplied by a Modulab Type II De-ionization System (Continental Water Systems, Sydney, Australia);

Slipicone® silicone release spray from DC Products, Mount Waverly, Australia; sodium dodecyl sulfate (SDS) from J. T. Baker Chemical Co., Phillipsburg, USA; methanol (HPLC grade) from Thermo Fisher Scientific Australia Pty. Ltd., Scoresby, Australia; Aerolizer® was supplied by Novartis Australia Pty. Ltd, North Ryde, Australia. Materials used to construct the containers included: polyethylene, polyvinyl chloride, Teflon, nylon (all Dotmar, North Ryde, Australia) and stainless steel (Mascot Steel, Mascot, Australia), details of which are described elsewhere (10).

Formulation Preparation

Amorphous SS was prepared by spray-drying an aqueous solution of 10% w/w SS (Büchi Mini Spray-Dryer B-290, Büchi Labortechnik, Flawil, Switzerland). The spray-dryer was connected to a Büchi Dehumidifier B-296 (in open loop, blowing mode). The operation conditions were as follows: liquid feed rate was 2.4 ml/min, inlet and outlet temperatures were 150°C and 96°C, respectively, aspiration rate was 38 m³/h and atomising air flow was 819 NI/h.

Crystalline SS was produced using a conditioning method described by Muhammed *et al.* (2010) (11). Briefly, a custom made high-pressure reaction vessel was loaded with amorphous spray-dried SS (1.5 g). Pressurized scCO₂ saturated with menthol was delivered using a high-pressure pump (A P50 series, Thar Technologies Inc., Pittsburgh, USA). Once the system was stabilized at 150 bar and 50°C, the reaction vessel was isolated to condition the spray-dried SS powder for a period of 12 h. During this period the vessel was stirred to prevent particle aggregation. After conditioning, residual menthol was purged from the system using neat CO₂ at 150 bar and 50°C at a constant flow rate of 10 ml/min for a period of 1.5 h. Finally, the system was depressurized and the powder was collected. Amorphous and crystalline SS powders were transferred to separate sealed containers, and stored under silica gel desiccant at 22°C until further analysis and processing.

Particle Size Distribution

Laser diffraction through a Sirocco 2000 dry powder feeder (Malvern Instruments, Worcestershire, UK) was used to determine particle size distribution. Triplicate samples of powder (approximately 10 mg) were dispersed at 4 bar. Measurement parameters were: obscuration of 0.3–10%, particle refractive index and absorption of 1.553 and 0.1, respectively; and the dispersant refractive index for air was 1.000. The diameters corresponding to the cumulative volume under 10, 50 and 90% were expressed as the d₁₀, d₅₀ and d₉₀, respectively. Span quantified the broadness of the size distribution and was defined as (d₉₀–d₁₀)/d₅₀.

Scanning Electron Microscopy

Scanning electron microscopy (SEM) was used to observe particle morphology. Samples were dispersed onto sticky carbon tape, mounted on SEM stubs, and sputter coated with approximately 15 nm thick gold using a K550X sputter coater (Quorum Emitech, Kent, UK). Images were obtained using a Zeiss Ultra Plus field emission SEM (Carl Zeiss SMT Ag, Oberkochen, Germany) at 5 kV using the secondary electron detector.

Atomic Force Microscopy

Three dimensional surface roughness was quantified using atomic force microscopy (AFM). A Veeco MultiMode™ SPM AFM, with Nanoscope IIIa controller and Nanoscope 5.31r1 software (Veeco Metrology Group Inc., Santa Barbara, USA), was used in TappingMode. The samples were dispersed onto Tempfix® (Plano GMBH, Wetzlar, Germany) and were imaged at a scan rate of 0.25 Hz using a Tap300AL-G cantilever (BudgetSensors, Sofia, Bulgaria). Areas of 512 nm × 512 nm with 512 × 512 sample points were imaged on three different individual particles. The root mean squared roughness (R_q) was obtained over the entire scanned area.

Surface Area Determination

Bulk particle specific surface area was determined using a Tristar™ II 3020 Surface Area Analyzer (Micromeritics, Norcross, USA) with nitrogen as the adsorbate gas. Triplicate samples (100 ± 10 mg) were degassed for approximately 24 h under nitrogen, to remove any pre-adsorbed gases and vapors on the surface. The specific surface area was calculated from the Brunauer, Emmett and Teller (BET) method using five point adsorption data in relative partial pressure (P/P_0) range of 0.06–0.20.

X-ray Diffraction

X-ray diffraction (XRD) was used to analyze sample crystallinity. An X-ray diffractometer (XRD-6000, Shimadzu Corporation, Kyoto, Japan) measured samples under ambient conditions using Cu K α radiation at 30 mA and 40 kV, with angular increments of 0.04° at 2 s per step covering a 2 θ range of 5–40°.

Gas Chromatography

An Agilent 7890A gas chromatograph (GC) coupled with a 7863 autosampler and flame ionization detection (FID) (Agilent Technologies, Santa Clara, USA) was used to measure the residual menthol. One μ L injections using splitless mode, with inlet and detector temperatures of 200°C and

250°C, respectively, were used. Analytes were separated by a HP-5 (30 m × 320 μ m × 0.25 μ m) column (Agilent Technologies, Santa Clara, USA) with 2 ml/min He carrier gas in constant flow mode. For standards, the GC oven temperature program was initiated at 80°C and held for 3 min, then ramped by 25°C/min to 200°C and held for 1 min. The total run time was 8.8 min. The same method was used to analyze samples, only it was held for a further 10 min at 200°C to ensure no impurities were carried over. The total run time for samples was 18.8 min. A calibration curve was constructed by serial dilution using freshly prepared standard solutions of menthol. Menthol was dissolved in *n*-hexane with concentrations from 0.001 to 1 mg/ml ($R^2 = 0.9999$). Prior to assay, triplicate samples of spray-dried and conditioned salbutamol sulfate with mass 5 ± 0.2 mg were dissolved in 5 ml of *n*-hexane and sonicated for 5 min.

Dynamic Vapor Sorption

A dynamic gravimetric water sorption analyzer (DVS Intrinsic, Surface Measurement Systems Ltd., London, UK) was used to determine moisture sorption profiles. Samples (approximately 10 ± 1 mg) were subjected to two sorption–desorption cycles from 0 to 90% RH in 10% RH steps at 25°C. The step-change criterion was determined by a percentage weight change $\leq 0.002\%$.

In Vitro Aerosol Performance and Characterization of Aerosol charges

A modified ELPI™ Classic (Dekati Ltd., Tampere, Finland) setup measured *in vitro* aerosol performance and inherent electrostatic charge. Aerosolization at 60 L/min was achieved by a Y-piece connected to a plastic unit dose collector and additional pump, as described by Kwok and Chan (4). The dose split ratios between the ELPI™ and unit dose collector for all dispersions was roughly 50:50, with no bias in either direction. Thus the aerosols could be considered evenly divided by the Y-piece, as previously reported.

Each impactor stage was sprayed with Slipicone® silicone prior to experiments to minimise particle bounce and re-entrainment. The solvent was allowed to evaporate before the unit was re-assembled. An Aerolizer® inhaler loaded with an empty capsule and fitted with a rubber adapter for airtight sealing was connected to a calibrated flow meter (TSI 3063, TSI Instruments Ltd., Shoreview, USA) to check and adjust the total flow rate to 60 L/min. The aerosol charges were measured and recorded using the Dekati ELPI™VI 4.0 software with the following settings: current range set at 400,000 fA, saving interval at 1 s, data correction unticked, trap off, and pressure drop adjusted to 100 mbar.

The ELPI™ was enclosed in a polycarbonate box with digital RH and temperature monitor (Thermo Fisher

Scientific Australia Pty. Ltd., Scoresby, Australia), and the electrometers were zeroed without flushing. When a stable zero baseline was obtained, approximately 5 ± 0.2 mg of sample was filled into a size 3 hydroxypropyl methylcellulose capsule (Vcaps®, Capsugel Australia Pty. Ltd., West Ryde, Australia) and loaded into the inhaler. Subsequently, the inhaler was inserted into the throat until the dose was completely emptied and all aerosol charges were measured from the dose. Immediately after dose sampling, the inhaler was reinserted and removed from the throat three times to generate blank signals. The mean of these readings was calculated and subtracted from the aerosol measurements to account for the disturbances in background electrical signals as a result of insertion of the inhaler to the throat. Triplicate dispersions were performed without gloves to simulate patient use.

Mass Assay

After aerosolization, drug that deposited on the device, capsule, adaptor, Y-piece, straight tube and each ELPI™ stage were exhaustively washed with 5 ml of de-ionized water. The unit dose collector and glass fiber filter were thoroughly washed with 10 ml of de-ionized water, and centrifuged (Minispin®, Eppendorf, Westbury, USA) at 13,400 rpm for 10 min. Aliquots of the samples were chemically assayed using high-performance liquid chromatography (HPLC). The mobile phase consisted of 1 g/L SDS dissolved in 60:40 v/v methanol:water, whereas the needle rinse consisted only of 60:40 v/v methanol:water. All mobile phases were filtered through a 0.45 μm polyamide filter membrane (Sartorius Stedim Biotech GmbH, Göttingen, Germany) before use. The Shimadzu HPLC system consisted of a SPD-20A UV detector set at a detection wavelength of 276 nm, LC-20AT pump and SIL-20A HT Autosampler coupled to LC Solution software (Shimadzu Scientific Instruments, Kyoto, Japan). Samples were injected (100 μL) into a Nova-Pak® C18 4 μm 4.6 \times 150 mm column (Waters, Milford, USA) at a flow rate of 1 ml/min, resulting in a retention time of 13 min. A calibration curve was constructed by serial dilution using freshly prepared standard solutions in de-ionized water at concentrations of 0.01 to 5 mg/ml ($R^2 = 0.999$).

Powder Tumbling and Net Charge Determination

Powder (500 ± 25 mg) was tumbled in containers made from different materials (polyethylene, polyvinyl chloride, Teflon, nylon and stainless steel). The containers had an approximate headspace of 13.4 cm^3 , which kept constant throughout the experiments and was filled with nitrogen. Powder was tumbled (Turbula mixer, Willy A. Bachofen AG Maschinenfabrik, Basel, Switzerland) at 42 rpm for 15 min under ambient conditions. Immediately after

tumbling, the powder was transferred to a Faraday pail housed in a polycarbonate box which allowed ambient conditions to be controlled within the range $50 \pm 5\%$ RH and $22 \pm 2^\circ\text{C}$. The magnitude and polarity of charge was measured by an electrometer (NanoCoulomb Meter 284, Monroe Electronics, New York, USA) ($n = 8$ for each container material).

Data Analysis

The ELPI measures the electrical current detected on each impactor stage over time. The *net charge* on a given stage was calculated to be the area under the curve in the current-*versus* time plot. Since the ELPI measures the current every second in femtoamperes, the area under the curve is the sum of the current values over the duration of aerosol charge detection. The dose-splitting ratio downstream from the Y-piece was calculated as a percentage of total mass from either the ELPI™ or unit dose collector to the total sum of both these components, with the ideal split ratio defined as 50:50. The *emitted dose* (ED) was defined as the total mass of drug recovered from components assayed excluding the capsule and inhaler. The *fine particle dose* (FPD) was defined as the total mass deposited on Stage 11 (with cut off diameter of 4.01 μm) and below divided by the fraction post Y-piece dose. The *fine particle fraction percentage loaded* ($\text{FPF}_{\text{Loaded}}\%$) was defined as the percentage of FPD in the loaded dose. The *charge-to-mass ratio* (q/m), also known as the *specific charge*, was given by the quotient of the *net charge* and drug mass on a particular impactor stage.

Statistical Data Analysis

Statistical analysis to evaluate differences between the means was conducted using unpaired two sample *t*-test for a 95% confidence limit (Prism, GraphPad Software Inc., La Jolla, USA). Differences with $p < 0.05$ were considered statistically significant.

RESULTS

Solid-State Characteristics

Production of amorphous spray-dried SS and crystalline scCO_2 conditioned SS resulted in powders with comparable particle size distributions (Table I). For simplification, amorphous spray-dried SS and crystalline scCO_2 SS will be referred to as amorphous SS and crystalline SS from herein.

The SEM images in Fig. 1 showed the spherical morphology for both amorphous and crystalline SS. Amorphous SS particles were smoother with dimpled surfaces, while crystalline SS had a rough and flaky surface.

Table 1 Laser Diffraction Size Distributions of Amorphous and Crystalline Salbutamol Sulfate (SS)

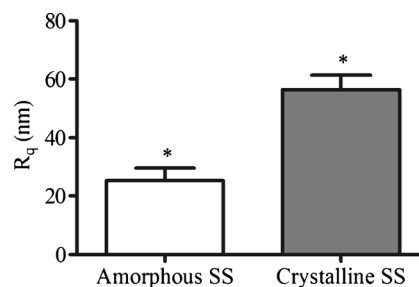
Formulation	Diameter (μm)			Span
	d_{10}	d_{50}	d_{90}	
Amorphous SS	0.74 (\pm 0.08)	2.82 (\pm 0.20)	5.99 (\pm 0.30)	1.86
Crystalline SS	0.78 (\pm 0.08)	2.71 (\pm 0.08)	5.64 (\pm 0.23)	1.79

Data presented as mean \pm standard deviation ($n=3$)

The obvious surface differences between amorphous and crystalline SS (Fig. 1) were quantified in terms of surface roughness and specific surface area. A significant difference in R_q of individual particles was observed (Fig. 2). Similarly, specific surface area of bulk samples increased from 2.11 (\pm 0.15) to 7.35 (\pm 0.04) m^2/g for amorphous and crystalline SS, respectively. The increased surface roughness suggested that crystallization occurred.

The XRD profiles in Fig. 3 show that amorphous SS exhibited a typical halo pattern while crystalline SS had prominent sharp peaks that largely overlapped with raw SS at various degrees 2θ . Furthermore, crystalline SS did not have any corresponding peaks with raw menthol, which suggested negligible menthol, if at all, was present in the final product. This was in agreement with the GC analysis that quantified menthol residue to be 0 and 0.0003 (\pm 0.0001) % (w/v) for amorphous and crystalline SS, respectively.

The different crystallinity between amorphous and crystalline SS was exemplified by the moisture sorption isotherms. The moisture uptake reached a maximum of 9.97% at 60% RH for amorphous SS, compared to 3.40% at 50% RH for

**Fig. 2** Root mean squared roughness (R_q) of amorphous and crystalline salbutamol sulfate (SS). Data presented as mean \pm standard deviation ($n=3$).

crystalline SS (Fig. 4). Amorphous SS showed rapid uptake of water up to 60% RH, followed by a slower rate of water release resulting in hysteresis. At the end of the first sorption–desorption cycle, a total weight gain of 1.61% was observed. This showed that amorphous SS underwent substantial re-crystallization of bulk amorphous regions when exposed to moisture. In contrast, crystalline SS exhibited a much smaller hysteresis which indicated that it had significantly less bulk amorphous regions, consistent with findings from the XRD. In both cases, no further weight changes were observed following the end of the first sorption–desorption cycle and all existing amorphous regions had completely re-crystallized.

Charge Measurements

This study characterized two different charging processes of amorphous and crystalline SS, namely, aerosolization and tumbling. The charge profiles generated from powder

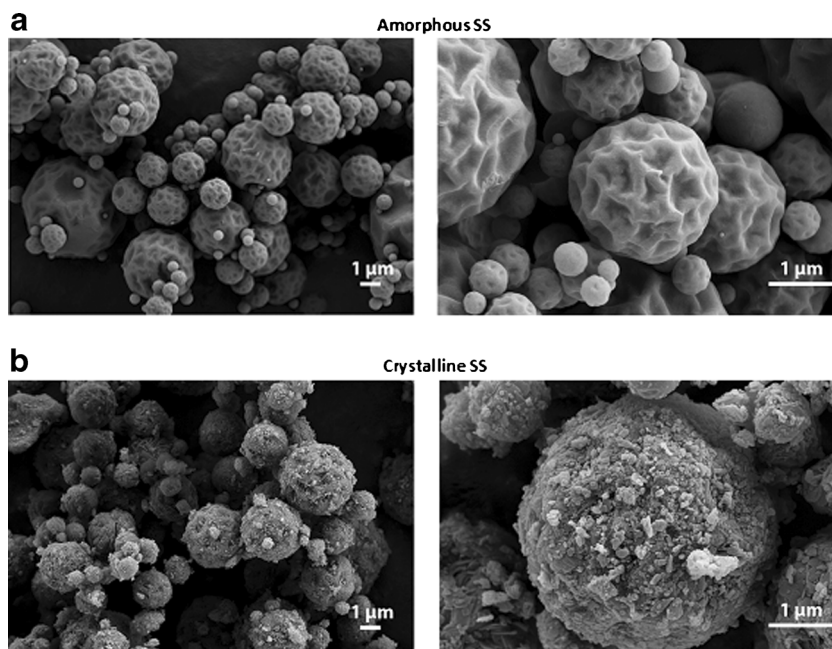
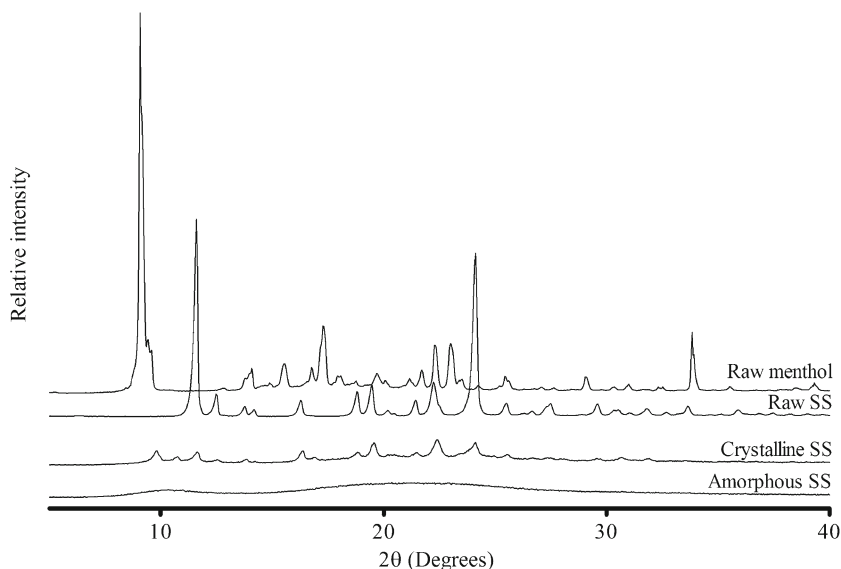
Fig. 1 Scanning electron microscopy of (a) amorphous and (b) crystalline salbutamol sulfate (SS). Magnifications at 15 K \times and 50 K \times magnification are on the left and right, respectively.

Fig. 3 X-ray diffractograms of raw menthol and raw, crystalline and amorphous salbutamol sulfate (SS).



dispersion through an Aerolizer® was measured by a modified ELPI™. *In vitro* electrostatic charge and mass deposition profiles are shown in Fig. 5. Both amorphous and crystalline SS exhibited a similar bipolar trend, with a change in polarity observed around the 1.60 μm cutoff diameter. Since the powders did not contain excipients, the charge measured in the submicron fractions must be due to the presence of highly charged SS nanoparticles. Overall, crystalline SS appeared to charge to greater magnitudes and may have more consistent charging and mass deposition. In addition, the mean emitted dose and FPF_{Loaded}% were higher for crystalline SS, but unlike the previous study (11) the improvement was not

statistically significant (Fig. 6). This could be attributed to batch-to-batch variation and a difference in impactor, flow rate, and dose delivered. Furthermore, specific charges were calculated (Table II) to account for differences in mass deposition. Significant differences in charging were observed between amorphous and crystalline SS, particularly on Stages 7 (with cutoff diameter of 0.615 μm) and below.

The tumbled powder charge was measured by a Faraday pail. In general, amorphous SS charged net positively with

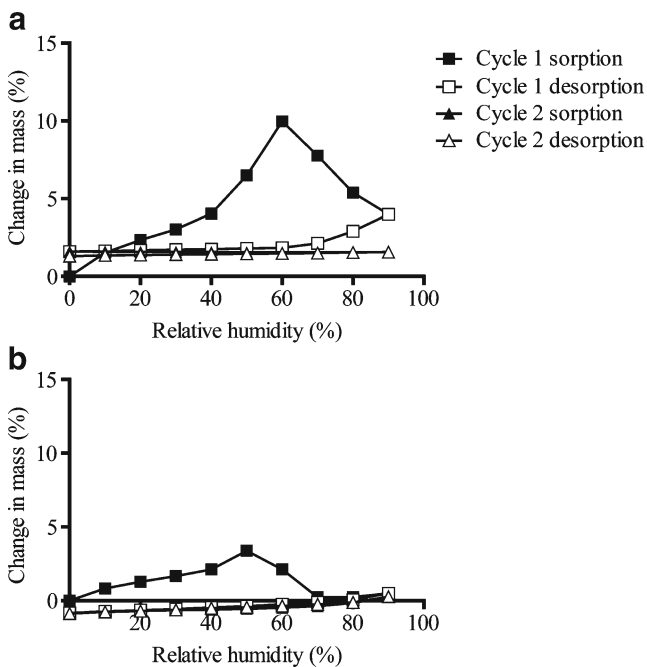


Fig. 4 Moisture sorption isotherms of (a) amorphous and (b) crystalline salbutamol sulfate.

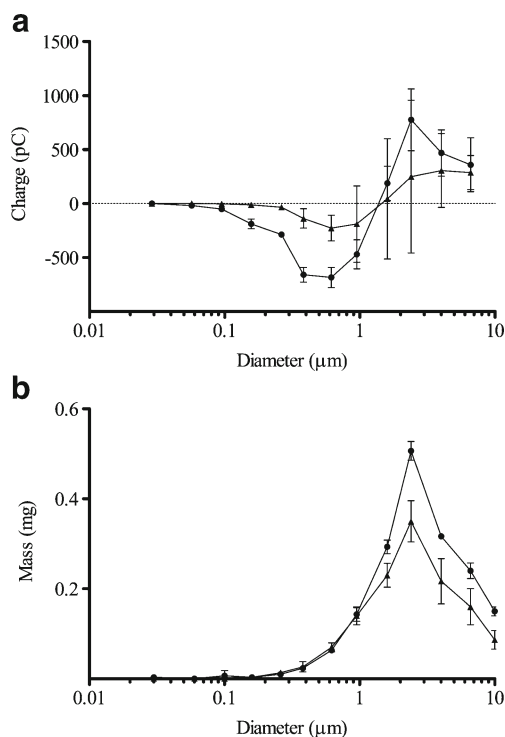
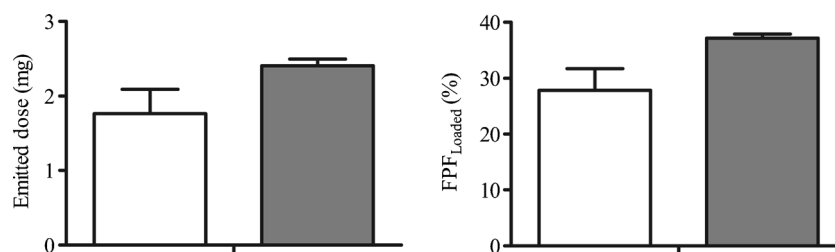


Fig. 5 Mean electrostatic charge and mass deposition profiles for (black triangle) amorphous and (black circle) crystalline salbutamol sulfate. Data presented as mean ± standard deviation (n=3).

Fig. 6 Mean emitted dose and fine particle fraction (% loaded) for amorphous (white) and crystalline (grey) salbutamol sulfate. Data presented as mean \pm standard deviation ($n=3$).



higher magnitudes, ranging from +15.0 to +26.6 nC/g. On the other hand, crystalline SS charged net negatively, except by the Teflon container, which charged the powder to +11.9 nC/g (Table III). When the specific charge was plotted against the work function of the container material, amorphous and crystalline SS resulted in correlation coefficients (R^2) of 0.03 and 0.71, respectively (Fig. 7). Since metals and insulators have fundamentally different charging mechanisms, on omission of the metal values the R^2 of crystalline SS improved to 0.94 (the value for amorphous SS was 0.02). Unlike the previous study by Adi *et al.* (10), the application of electron donating/accepting properties (γ^-/γ^+) showed no correlation and could not adequately explain the results in the present study. When the specific charge was plotted against γ^-/γ^+ , R^2 values for amorphous and crystalline SS corresponded to 0.21 and 0.55, respectively (plot not shown).

DISCUSSION

This study focused on two charging processes of amorphous and crystalline SS. The charge profile generated following aerosolization from an inhaler was compared to the net charge generated following tumbling in different containers made of single materials. Due to differences in the nature of contact charging, i.e. a complex interplay between the capsule, powder and inhaler during aerosolization in comparison to the tumbling motion of powders in containers made of a single material, the magnitude and polarity of charge between the two processes are not comparable. However, these studies have introduced new mechanistic trends in the charging of amorphous and crystalline SS.

The dispersion of crystalline SS appeared to have potentially more consistent charging and mass deposition. The higher variation in the aerosol charges for amorphous SS may be due to the ill-defined surface nature (i.e. molecular arrangement) of the amorphous particles, leading to variable charge transfer behavior. The tumbling studies of crystalline SS showed a significant correlation between net charge and work function, whereas the amorphous SS showed no such correlation. This difference may be a reflection of the long-range molecular order of the crystal lattice leading to predictable charging in crystalline SS, in comparison to the random order in amorphous SS. In addition, the polarity of charging could be explained by the arrangement of SS molecules in the crystal lattice. Molecular modeling showed that the dominant crystal surface of SS contains sulfate counter-ions (12). The presence of more electronegative sulfate counter-ions on the surface of ordered crystalline SS (than would otherwise be by random arrangement as in the case of amorphous SS), would result in a higher work function for the crystalline SS surface. Work function refers to the minimum energy required to remove an electron from the surface of a solid to an infinitely far position. In theory, a higher work function means that the surface is less likely to lose electrons (i.e. tends to accept electrons). Hence, the mean charge of crystalline SS for all container materials is much less positive than in the case of amorphous SS.

This study also highlighted an important gap in the fundamental theory of charging. Two charging concepts, namely work function and γ^-/γ^+ , were applied in the present study. Work function is a concept derived from metal-metal contact charging that hypothesized electron transfer occurs from the material with lower work function to that with a

Table II Specific Charges ($\mu\text{C/g}$) of Amorphous and Crystalline Salbutamol Sulfate (SS) on Impactor Stages with Detectable Drug Mass

Stage cutoff diameter (μm)	4	5	6	7	8	9	10	11	12
	0.157	0.263	0.383	0.615	0.951	1.60	2.40	4.01	6.61
Amorphous SS	-5.73 (0.37) ^a	-2.47 (0.62) ^b	-3.01 (1.95) ^c	-2.00 (1.03) ^d	-0.81 (1.51)	0.11 (1.36)	0.42 (1.19)	0.87 (0.98)	1.17 0.65
Crystalline SS	-94.29 (22.19) ^a	-20.55 (1.65) ^b	-14.33 (1.48) ^c	-6.00 (0.81) ^d	-2.01 (0.57)	0.46 (0.39)	1.30 (0.48)	1.34 (0.61)	1.47 1.02

Data presented as mean \pm standard deviation in parenthesis ($n=3$). Means with a common letter in superscript are statistically significant ($p \leq 0.05$)

Table III Specific Charges (nC/g) of Amorphous and Crystalline Salbutamol Sulfate (SS) Generated by Tumbling in Containers Made of Different Materials

Container material	Work function (eV) ^a	Specific charge (nC/g)	
		Amorphous SS	Crystalline SS
Non-metal	Polyethylene	4.9	15.02 (2.14) / -4.45 (4.19)
	Nylon	4.4	18.62 (5.09) / -5.65 (1.76)
	Polyvinyl chloride	5.1	26.49 (5.31) / -13.07 (0.90)
	Teflon	5.8	26.61 (1.85) / 11.88 (2.52)
Metal	Stainless steel	5.15	26.22 (5.94) / -12.10 (2.52)

Data presented as mean \pm standard deviation ($n=8$)

^aWork function values were obtained from (10)

high work function until the electron energies equilibrate (13). Alternatively, γ^-/γ^+ is a parameter related to the polar component of surface energy which is derived from the acid/base properties. Since electrostatic charge is a surface phenomenon, this concept has also been applied to explain charging that arises from different polar interactions between particles and material surfaces (10). Unlike the previous findings, γ^-/γ^+ showed no correlation with the tumbled charges and could not adequately explain the results in the present study. Rather, the work function model provided greater insight.

Despite its ubiquitous nature, triboelectrification is complex and current knowledge on the fundamental mechanisms remains limited. Although the literature reports a number of theoretical models on solid charging, yet no single model can successfully explain and predict charging. This is reflected in the observation that the results of this study fitted the work function model but not the surface energy one. The charging trends may be dependent on the constituent of the particles, construction material of the inhaler/container, the mode of charging, and environmental conditions. Thus, the study of triboelectrification is still at the hypothesis formation stage, and more experimental data are needed to further understand this phenomenon and its fundamental mechanisms.

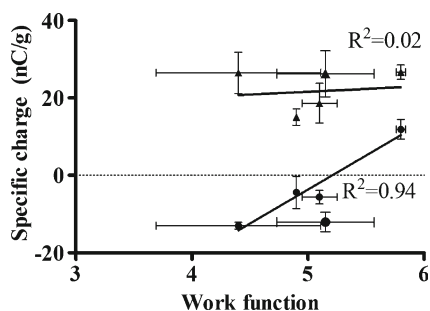


Fig. 7 Correlation between specific charge and work function for (black triangle) amorphous and (black circle) crystalline salbutamol sulfate. Data presented as mean \pm standard deviation.

Several limitations in the present study should be noted. First, the individual electrometers connected to each impactor stage of the ELPI™ impactor could only give net charge measurements, such that the bipolarity within each size fraction could not be discerned. Second, completely crystalline SS could not be produced due to limitations with the production method. Prolonged conditioning yielded increasingly crystalline particles that lost sphericity and became aggregated. Nonetheless, the XRD and DVS data show the powders obtained had sufficiently different crystallinity for the purpose of this study. Third, surface roughness may also play a role in the generation of charge. The relatively smooth surfaces of amorphous SS is likely to have homogeneous charge distribution, whereas the rougher crystalline SS tends to have charge concentrated at the asperities (14). As a result, following violent collisions during aerosolization, charge transfer in crystalline SS could give rise to higher charge magnitudes. Unfortunately, whilst the sphericity of crystalline SS particle shape was maintained, the surface roughness (hence surface area) increased significantly. However, it is very difficult to vary crystallinity without affecting the morphology because crystallization necessitates the re-arrangement of molecules into orderly lattices. Therefore, future studies could explore the role of surface morphology in electrostatic charging of DPI formulations. Finally, the results obtained here only apply to amorphous and crystalline SS. A difference in crystallinity may potentially affect consistency in charging and aerosol performance, but additional extensive research is needed on multiple formulations and inhaler/container materials to confirm the trends.

CONCLUSION

This is the first study that has investigated the effect of crystallinity on the electrostatic charge behavior of inhalable micron-sized spherical drug particles with well-defined particle size distribution. Upon aerosolization from an inhaler, crystalline SS appeared to show more consistent charging and mass deposition. Crystalline SS from the tumbling study showed a significant correlation between net charge and work function, whereas amorphous SS showed no such correlation. Triboelectrification is complex thus no single current theoretical charging model could explain the results totally. More work in this area is needed to increase our understanding in the fundamentals of charging. The knowledge gained may assist in the development of optimized inhaled products.

ACKNOWLEDGMENTS AND DISCLOSURES

The authors thank Ms. Ellen Braybon from Faculty of Chemistry, University of Sydney, for providing instrumental

facilities and assistance for GC analysis; the Australian Microscopy & Microanalysis Research Facility, University of Sydney, for providing facilities for SEM imaging; Mr. David Cipolla from Aradigm Corporation for feedback on the manuscript, and Dr. Dai Hibbs from the Faculty of Pharmacy, The University of Sydney, for valuable discussions. This research was supported under Australian Research Council's Discovery Projects funding scheme (project numbers DP120102778 & 110105161).

REFERENCES

1. Wong J, Chan H-K, Kwok PCL. Electrostatics in pharmaceutical aerosols for inhalation. *Ther Deliv.* 2013;4:981–1002.
2. Byron PR, Peart J, Staniforth JN. Aerosol electrostatics I: properties of fine powders before and after aerosolization by dry powder inhalers. *Pharm Res.* 1997;14:698–705.
3. Telko MJ, Kujanpaa J, Hickey AJ. Investigation of triboelectric charging in dry powder inhalers using electrical low pressure impactor (ELPI). *Int J Pharm.* 2007;336:352–60.
4. Kwok PCL, Chan HK. Effect of relative humidity on the electrostatic charge properties of dry powder inhaler aerosols. *Pharm Res.* 2008;25:277–88.
5. Young P, Sung A, Traini D, Kwok P, Chiou H, Chan H-K. Influence of humidity on the electrostatic charge and aerosol performance of dry powder inhaler carrier based systems. *Pharm Res.* 2007;24:963–70.
6. Karner S, Anne Urbanetz N. The impact of electrostatic charge in pharmaceutical powders with specific focus on inhalation-powders. *J Aerosol Sci.* 2011;42:428–45.
7. Kwok PCL, Chan HK. Electrostatics of pharmaceutical inhalation aerosols. *J Pharm Pharmacol.* 2009;61:1587–99.
8. Murtomaa M, Harjunen P, Mellin V, Lehto V-P, Laine E. Effect of amorphicity on the triboelectrification of lactose powder. *J Electrostat.* 2002;56:103–10.
9. Kwok PCL, Chan HK. Solid forms and electrostatic properties of salbutamol sulfate. In Dalby R, editors. *Respiratory drug delivery*, vol. 3, River Grove; 2008, pp. 919–22.
10. Adi H, Kwok PCL, Crapper J, Young PM, Traini D, Chan H-K. Does electrostatic charge affect powder aerosolisation? *J Pharm Sci.* 2010;99:2455–61.
11. Muhammad SA, Langrish T, Tang P, Adi H, Chan H-K, Kazarian SG, *et al.* A novel method for the production of crystalline micronised particles. *Int J Pharm.* 2010;388:114–22.
12. Xie S, Poornachary SK, Chow PS, Tan RBH. Direct precipitation of micron-size salbutamol sulfate: new insights into the action of surfactants and polymeric additives. *Cryst Growth Des.* 2010;10:3363–71.
13. Gallo CF, Lama WL. Classical electrostatic description of the work function and ionization energy of insulators. *IEEE Trans Ind Appl.* 1976;12:7–11.
14. Zeng XM, Martin GP, Marriott C. *Particulate interactions in dry powder formulations for inhalation.* London: Taylor and Francis; 2003.